 doi:10.20944/preprints201902.0192.v1

Optimization of Process Parameters for Anti-Glare Spray Coating by Pressure-feed Type Automatic Air Spray Gun Using Response Surface Methodology

Yu-Hui Huang[1*] Lung-Chuan Chen[2*] Huann-Ming Chou[3]

[1] Graduate School of Mechanical and Energy Engineering, Kun Shan University
[2] Department of Materials Engineering, Kun Shan University
[3] Department of Mechanical and Energy Engineering, Kun Shan University

Abstract:

The process of preparing anti-glare thin films by spray-coating silica sol-gel to soda-lime glass was exclusively and statistically studied in this paper. The effects of sol-gel delivery pressure, gas transport pressure, and displacement speed on the gloss, haze, arithmetic mean surface roughness (Ra) and total transmittance light (TTL) were analyzed. The experimental results indicate that the factors of sol-gel delivery pressure, air transport pressure, and displacement speed exhibits significant effect on the haze, gloss, and Ra. In contrast, the variation of TTL with these three factors are insignificant. Because the anti-glare property is predominantly determined by low gloss and high haze, therefore, we aim to minimize gloss and maximize haze to achieve high anti-glare. Response Surface Methodology (RSM) was employed to analyze the main and interactions effect of the three factors through a quadratic polynomial equation by. The analysis of variance (ANOVA) and R^2 analysis confirm the adequacy of the semi-empirical equation. The RSM predict the lowest gloss and highest haze are 9.2 GU and 59.3%, corresponding to the (sol-gel delivery pressure, air-transport pressure, displacement speed) of (250, 560, 140) and (260, 600, 20), respectively. Comparing the predicted optimal data with the real experimental results confirms the applicability of the mathematical model. The results of this study provide a crucial basis for subsequent production of anti-glare glass in response to market demand.

Keywords: Anti-Glare, Spray-coating, Gloss, Haze, Response Surface Methodology

Preprints (www.preprints.org) | NOT PEER-REVIEWED | Posted: 20 February 2019 doi:10.20944/preprints201902.0192.v1

Introduction

With the huge demand for smart phones, it is almost a "everyone equipped with a cell-phone" situation. The consumers are paying more and more attention to smart phones. In terms of portability that they are not only request to mobile phones that are light with thin and good texture. Mainly, the requirements for entertainment are increasing day by day, and the demand for visual and operational convenience is also relatively increased, which in turn drives the smart phone technology to be constantly updated, making the application field are more extensive. Anti-Glare treatment could reduce the high light intensity and glare caused by excessive concentration of light, thereby improving the user's comfort for cover lens, which was shown schematically in Figure1. Surface atomization process is widely applied to prepare anti-glare glass, and the methods of nano-particle coating [1-3], solution etching [4-5] and sol-gel coating [6-7] are commonly involved to generate anti-glare structures. Although nano-particles can be easily coated on glass substrates by spray coating, spin coating, and dip coating techniques, however, there are still some technical challenges in the uniformity of nano-particle distribution. Although it has been over 30 years that the spray-coating process with the sol-gel particles as the industry's main method for anti-glare surface treatment, however, till now, the optimization conditions of these processes are still far from clear because they are affected by more than 50 main variables and their interactions [8]. Therefore, the key equipment of the precision coating process and the optimization of the operating parameters are the key points for improving the performance of the spraying system. Therefore, based on the earlier research [17], this study will adopt the response surface methodology (RSM) experimental design to explore the regulation of anti-glare sol-gel spray parameters and their optimization. Finally, an empirically regression equation was obtained to describe the quantitative effects of the operating parameters on the anti-glare.

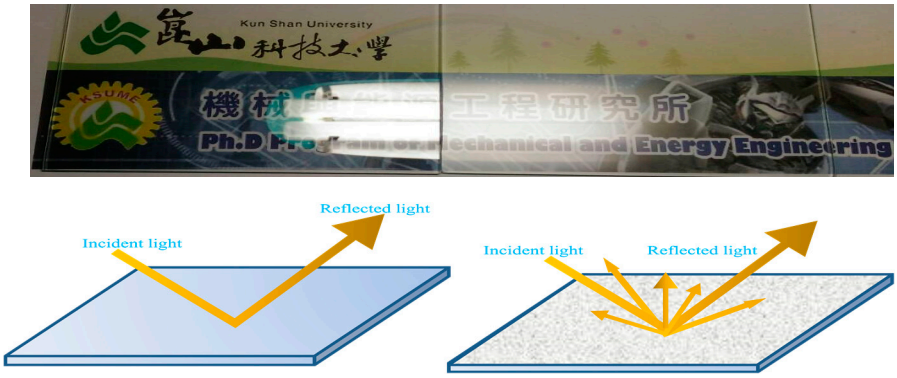

normal glass anti-glare glass

Figure 1. The show normal glass and anti-glare glass product, and light reflection schematic diagram

Preprints (www.preprints.org) | NOT PEER-REVIEWED | Posted: 20 February 2019 doi:10.20944/preprints201902.0192.v1

2. Materials and Methods

2.1. Materials

High purity tetraethoxysilane (TEOS) and methyltrimethoxysilane (MTMS) were purchased from Evonik (Germany). Nitric acid (EP) was purchased from Union Chemical Works. Methanol were all of 99.9% purity and obtained from Shiny Chemical Industry Co. Purified Water (> 18MΩcm) was used in this study.

2.2. Fabrication of Anti-glare Sol-gel

The anti-glare Sol-gel formulation was as described by Huang et al. [17] and modified as follows. The desired amounts of TEOS, MTMS, Methanol, Purified Water and nitric acid were added into a 1L glass container and then magnetically agitated for 24 h at 25℃. Then, the sol-gel solution was aged at 4℃ for 4 days. The molar ratio of TEOS: MTMS: Methanol: HNO_3: H_2O was 1: 0.39: 8.39: 0.02: 5.17.

2.3. Preparation of Anti-Glare Film Layer

The glass substrates with a diameter of 100×100 mm and thickness of 3 mm were ultrasonically cleaned at 50 ℃ for 30 min and then baked at 80 ℃ for 1 h. The prepared silica sol-gel samples were deposited onto the cleaned substrates through an automated spray coating system, which was shown schematically in Figure2. The operating variables of deliver pressure, provided pressure of transport air, and the spray gun displacement speed were investigated during the sol-gel deposition under one-pass spray operation conditions. The obtained silica anti-glare film/glass samples were heated at 180℃ for 1 h. In this work, the Auto-spray gun (S-710AD) was purchased from Guan Piin Painting Technology Co., Ltd. (Taiwan). The environmental temperature/humidity was well controlled at 25 ℃/ 40%.

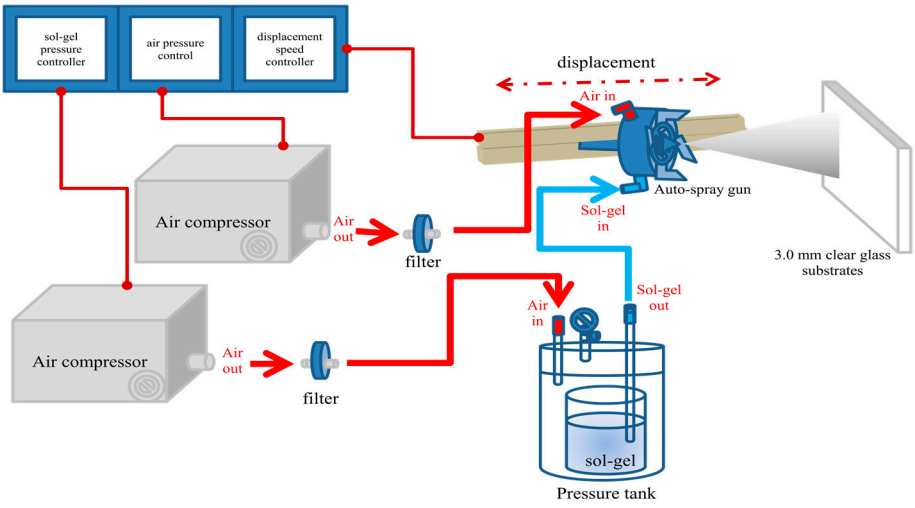

Figure 2. Schematic diagram of the anti-glare thin film production by auto-spray system.

Preprints (www.preprints.org) | NOT PEER-REVIEWED | Posted: 20 February 2019 doi:10.20944/preprints201902.0192.v1

2.4. Characterization

The morphology of the anti-glare thin films was observed using the digit microscope (UPG670, UPMOST technology corp., Taipei City, TW). The surface anti-glare property (gloss & haze) of the thin films were measured by the BYK micro-TRI-gloss device (BYK Additives & Instruments Company, Bavarian, GER), and WGT-S haze meter (Lab-think Instruments Company, Jinan, CN),and the totally transmitted light (TTL) were measured using the HMT MFS-630 angle-adjustable optical measurement analyzer (Hong-Ming Technology Company, New Taipei City, TW). Finally, the arithmetical mean deviation of the surface roughness profile (Ra) was measured using the Surface Roughness Tester (TR-200, Peking, SAIBORUIXIN).

2.5. Statistical Response Surface Methodology Analysis and Experimental Design

Experimental design is a strategy to study the main and interacted effects of the operating variables by simultaneously changing multiple variables at one run instead of only changing one variable at one run in the traditional model, which can significantly reduce the test numbers and studied time. Response surface methodology (RSM) is a kind of experimental design and is to optimize multiple responses by beginning with separate optimization of each response, followed by overlaying contour and surface plots of each function, and then to the derivation of complex functions aiming to simultaneously optimize all responses [9~11]. Following our previous experimental results [17], we attempt to optimize the response gloss (Y_1) and haze (Y_2) of the anti-glare thin from the independent variables of delivered pressure (X_1), the provided pressure of transport air (X_2), and the spray gun displacement speed(X_3) using the three-factor central composite experimental design. For each factor was examined at five levels, coded −1.68, −1, 0, 1 and 1.68, the ranges and the levels of the variables investigated were shown in Table 1.

Table 1. Experiment range and coded levels of the independent variables

Independent Variable	Symbol	Code Level				
		-1.68	-1	0	+1	+1.68
sol-gel pressure (kPa)	X_1	135.2	176	236	296	336.8
air pressure (kPa)	X_2	272	340	440	540	608
displacement speed (mm/sec)	X_3	196	230	280	330	364

Preprints (www.preprints.org) | NOT PEER-REVIEWED | Posted: 20 February 2019 doi:10.20944/preprints201902.0192.v1

The coded values were obtained according to eq. (1), where $\chi_{i'}$, χ_i, and $\Delta\chi_i$ represent independent variable coded value, independent variable real value, and the step change of the real value corresponding to a variation of a unit for the dimensionless value of the variable i, respectively.

$$\chi_{i'} = \frac{(\chi_i - \chi_0)}{\Delta\chi_i} \qquad (1)$$

According to the three-factor design, sixteen experiments combination were used and with two repetitive runs at the central point for estimation of the pure error sum of squares were employed. Table 2 shows the range of variables and the experimental design.

Table 2. Experimental results of the central composite design

No.	Sol-Gel pressure (kPa)	Air pressure (kPa)	Displacement speed (mm/s)	Gloss (GU)	Haze (%)	Ra (μm)	TTL (%)
1	176	340	230	32.8	27.3	0.34	93.7
2	176	340	330	42.0	22.3	0.26	93.3
3	176	540	230	23.5	35.6	0.35	94.0
4	176	540	330	31.0	28.6	0.26	93.5
5	296	340	230	70.2	15.1	0.24	92.1
6	296	340	330	79.8	8.5	0.22	92.5
7	296	540	230	20.8	37.6	0.49	92.7
8	296	540	330	45.6	22.8	0.29	93.3
9	135.2	440	280	38.6	26.4	0.19	92.7
10	336.8	440	280	60.5	21.9	0.36	93.0
11	236	272	280	68.2	11.1	0.31	92.3
12	236	608	280	28.5	29.2	0.39	93.1
13	236	440	196	18.7	39.8	0.58	93.6
14	236	440	364	42.3	18.5	0.27	92.6
15(C)	236	440	280	25.1	31	0.35	93.3
16(C)	236	440	280	26	32	0.35	93.5

Preprints (www.preprints.org) | NOT PEER-REVIEWED | Posted: 20 February 2019 doi:10.20944/preprints201902.0192.v1

Usually, the response value can be predicted by fitted to the following second order polynomial Equation (2) [12, 13]:

$$Y = a_0 + a_1X_1 + a_2X_2 + a_3 + +X_3 + a_{12}X_1X_2 + a_{13}X_1X_3 + a_{23}X_2X_3 + a_{11}X_1^2 + a_{22}X_2^2 + a_{33}X_3^2 \quad (2)$$

where Y represents the dependent variable; X_1, X_2 and X_3 represents the independent variables; a_0 represents the regression coefficient at the center point; a_1, a_2 and a_3 represents the linear coefficients; a_{12}, a_{13} and a_{23} represents the second order interaction coefficients; and a_{11}, a_{22} and a_{33} represents the quadratic coefficients. The optimum operating conditions can be estimated through three-dimensional response surface plots of the independent variables and each dependent variable. All relevant experimental data regression analysis and plotting were performed using the "Statistica" statistical suite software. The coefficients can be regressed using ANOVA ($p < 0.05$), which was used as a tool to check the significance of each of the coefficients, and the R^2 value can be used to determine the fitting quality of the obtained results associated with the proposed model. The three-dimensional surface plots can be adopted to account for the effects of the independent variables on the response variables.

3. Results and Discussion

- 3.1 Evaluation of the most substantial factors affecting anti-glare

The independent variables of sol-gel deliver pressure, the air transport pressure, and spray gun displacement speed are supposed to exhibit significant influences on the property of anti-glare. Therefore, these variables were systematically studied using the traditional method by varying one factor at a time and keeping other variables unchanged. Figure 3a exhibits the effect of sol-gel deliver pressure on TTL and haze, and Figure 3b displays the trends of gloss and Ra. The TTL slowly increases from 91.2 to 92.8% as the sol-gel pressure increases from 60 to 210 kPa, meanwhile a sharp raise of the haze from 2.8 to 28.0% is observed in the same region of sol-gel deliver pressure. Both the TTL and haze reach the plateau values as the sol-gel deliver pressure increases to 210 kPa, and then they decrease with further increasing in sol-gel pressure. In contrast, the gloss initially decreases with increasing of sol-gel pressure until 210 kPa, after that it increases as the sol-gel deliver pressure further increases. On the other hand, the Ra value increases with increasing sol-gel pressure ranging from 60 to 600 kPa. Increasing sol-gel pressure implies the increment of the deposited thickness of the thin film, which is beneficial to reduce gloss and boost haze and TTL.

Preprints (www.preprints.org) | NOT PEER-REVIEWED | Posted: 20 February 2019 doi:10.20944/preprints201902.0192.v1

Table 3. Effects of the sol-gel deliver pressure on the gloss, haze, Ra, and TTL of the anti-glare thin films with air transport pressure and displacement speed of 300kPa and 300 mm/s, respectively.

No.	Sol-Gel pressure (kPa)	Air pressure (kPa)	Displacement speed (mm/s)	Gloss (GU)	Haze (%)	Ra (μm)	TTL (%)
1	60	300	300	130.5	2.8	0.074	91.2
2	120	300	300	67.6	15.3	0.194	91.7
3	210	300	300	25.6	28.0	0.398	92.8
4	300	300	300	28.8	26.3	0.427	92.5
5	600	300	300	89.2	8.2	0.873	88.8

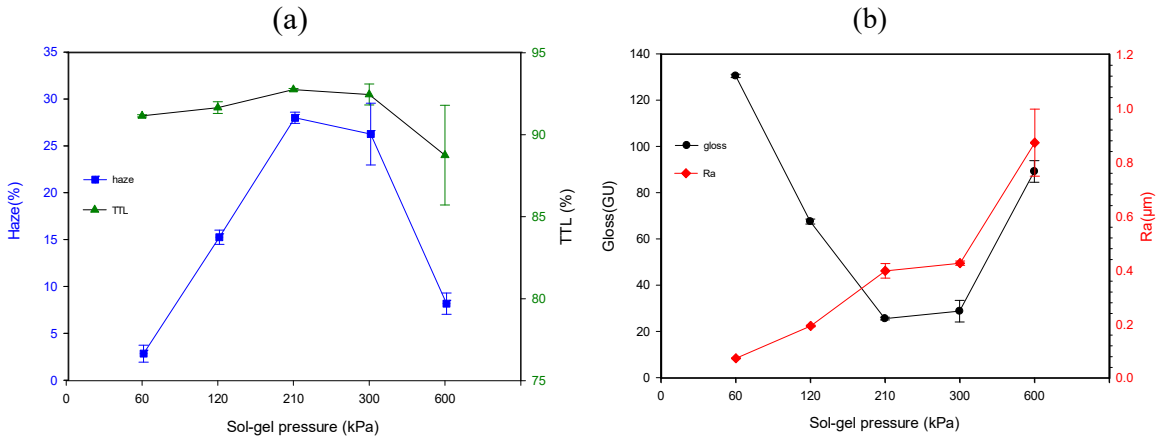

Figure 3. The influence of sol-gel deliver pressure on (a)TTL and haze (b)gloss and Ra with air transport pressure and displacement speed of 300kPa and 300 mm/s, respectively.

The microstructure of anti-glare film is characterized by digit microscope and is shown in Figure 4. It can be seen from the micrograph of 185 times magnification (90◦ and 25◦) that increasing sol-gel pressure results in a coarser surface and larger particle size of the anti-glare thin film, which in turn enhances its scattering effect. In addition, based on the previous research [17], the deposited sol-gel particles can form a low-refractive SiO_2 film layer and improve the transmittance when the film thickness increases [17]. However, excess sol-gel pressure may cause the film thickness exceeding the optimum one and generate a thick, smooth, and transparent structure, hindering the anti-glare efficiency. Furthermore, the thin film layers may grow too

Preprints (www.preprints.org) | NOT PEER-REVIEWED | Posted: 20 February 2019 doi:10.20944/preprints201902.0192.v1

thick and cause the formation of cracking (Figures 4(e), 4(j)), as a result that the gloss value will increase, and the haze and transmittance lower accordingly.

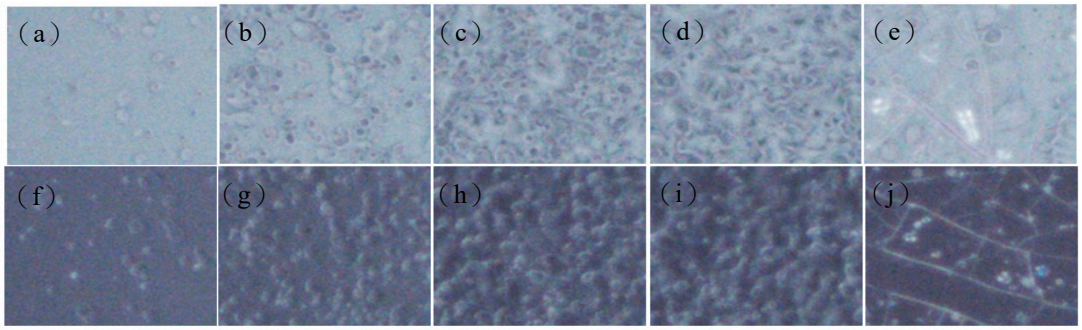

Figure 4. The digital microscope pictures of microstructure morphology of anti-glare samples by different sol-gel delivery pressure: (a) 60 kPa (90◦), (b) 120 kPa (90◦), (c) 210 kPa (90◦), (d) 300 kPa (90◦), (e) 600 kPa (90◦), (f) 60 kPa (25◦), (g) 120 kPa (25◦), (h) 210 kPa (25◦), (i) 300 kPa (25◦), and (j) 600 kPa (25◦).

Figures 5a and 5b show the effects of air transport pressure on gloss, haze, TTL, and Ra with the sol-gel deliver pressure and displacement speed are kept at 120k Pa and 300 mm/s, respectively. The results indicate that increasing air transport pressure causes decrements of gloss and Ra, and increments of haze and TTL.

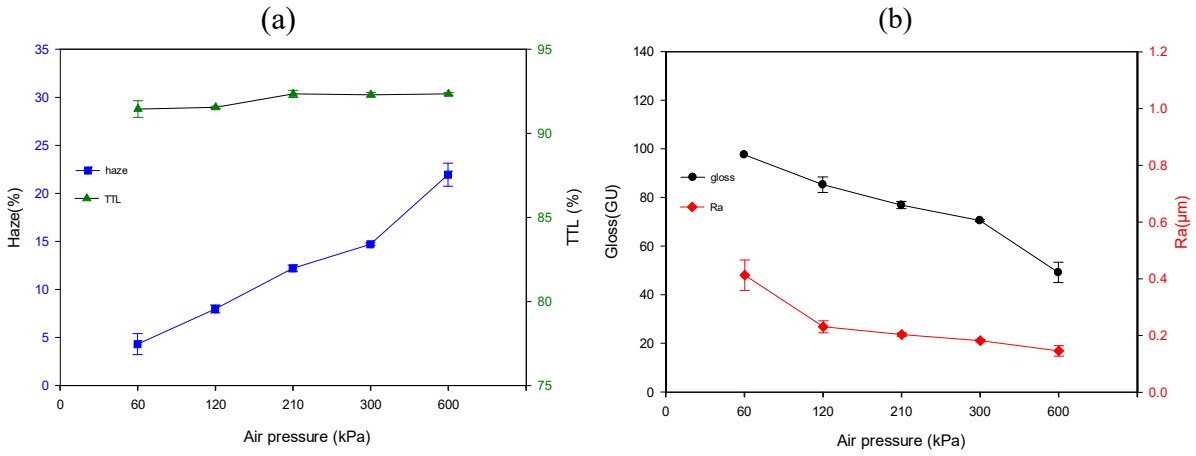

Figure 5. The influence of air transport pressure on (a) Haze and TTL and (b)gloss and Ra with the sol-gel deliver pressure and displacement speed of120k Pa and 300 mm/s, respectively.

The microstructure of anti-glare film is studied by digital microscope and is shown in Figures 6. It can be seen from the micrograph of 185 times magnification

Preprints (www.preprints.org) | NOT PEER-REVIEWED | Posted: 20 February 2019 doi:10.20944/preprints201902.0192.v1

(90°and 25°) that increasing air transport pressure can produce smaller particles to construct the anti-glare films due to the intensification of atomization. These tiny particles are favorable of generating anti-glare property and reducing surface roughness.

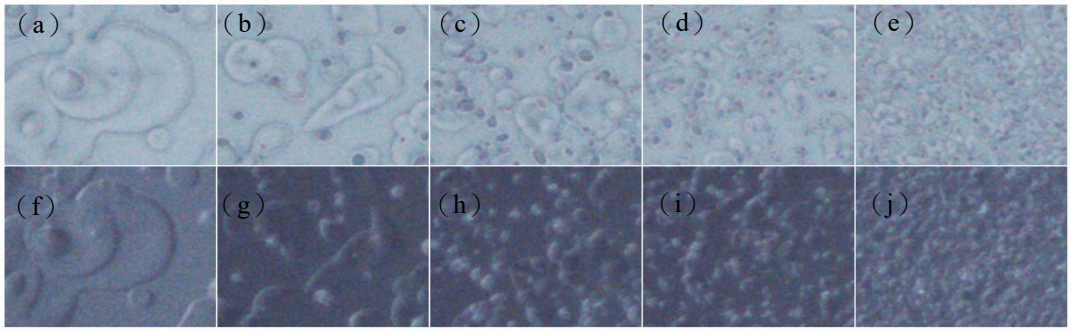

Figure 6. The digital microscope pictures of microstructure morphology of anti-glare samples by different air transport pressure (a) 60 kPa (90°), (b) 120 kPa (90°), (c) 210 kPa (90°), (d) 300 kPa (90°), (e) 600 kPa (90°), (f) 60 kPa (25°), (g) 120 kPa (25°), (h) 210 kPa (25°), (i) 300 kPa (25°), and (j) 600 kPa (25°).

Figure 7a and 7b demonstrate the effect of the spray displacement speed on gloss, haze, TTL, and Ra while the sol-gel and air transport pressures are kept at 120 kPa and 300 kPa, respectively. The experimental results exhibit that increasing spray displacement speed results in significant increment of gloss and decrease of haze, while the Ra and TTL insignificantly lower with the increase of displacement speed varying in the range of 170 and 500 mm/s.

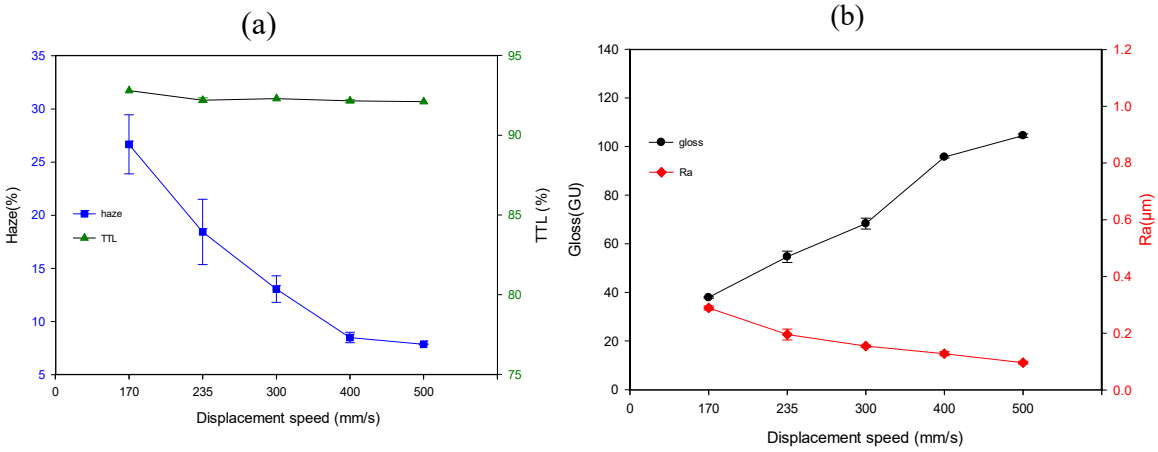

Figure 7. The influences of spray displacement speed on (a)haze and TTL, and (b)gloss and

Preprints (www.preprints.org) | NOT PEER-REVIEWED | Posted: 20 February 2019 doi:10.20944/preprints201902.0192.v1

Ra with the sol-gel deliver and air transport pressures of 120 kPa and 300 kPa, respectively.

Figure 8 explores the microstructures of the anti-glare thin film varied with the displacement speed. It can be seen from the micrograph of 185 times magnification (90° and 25°) that many voids occur and the particles distribution is bumpy. Therefore, the development of anti-glare property with increasing of displacement speed is irrelevant.

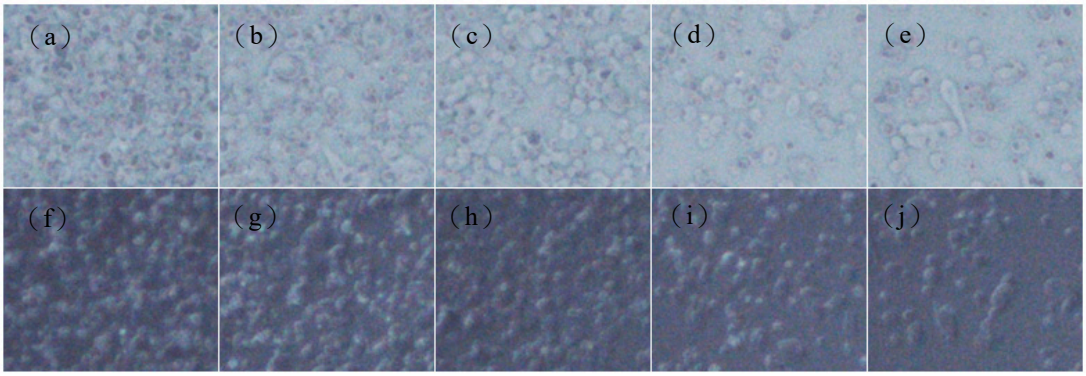

Figure 8. The digital microscope pictures of microstructure morphology of anti-glare sample by different the spray gun displacement speed (a) 170 mm/s (90°), (b) 235 mm/s (90°), (c) 300 mm/s (90°), (d) 400 mm/s (90°), (e) 500 mm/s (90°), (f) 170 mm/s (25°), (g) 235 mm/s (25°), (h) 300 mm/s (25°), (i) 400 mm/s (25°), and (j) 500 mm/s (25°).

Accordingly, the aforementioned single-variable studies clearly indicate that these three operating parameters will exert a significant effect on the anti-glare properties of the thin film. Therefore, a statistically experimental design based on the central composite design and response surface methodology will be conducted to find out the optimal operating conditions for optimizing anti-glare property.

3.2 Statistical Analysis

Greassham et al. [14] and Box et al. [15] pointed out that the experimental design method can provide an effective method to study the influence of operating parameters on the objective function to obtain the optimal conditions with the advantages of reduce cost and labor saving. This study employed the RSM experimental design method to find the optimum spray conditions to produce

Preprints (www.preprints.org) | NOT PEER-REVIEWED | Posted: 20 February 2019 doi:10.20944/preprints201902.0192.v1

anti-glare glass. In general, the anti-glare property predominantly relies on gloss and haze. Therefore, this study uses a 3-factor center mixed experimental design, with a midpoint (0,0,0) two replicates, and with other combinations to sixteen sets of experiments. The experimental results based on the central composite design are summarized in Table 2. According to the establishment of experimental data and multi-regression data matching techniques, the relationship and mathematical mode of the interaction effect between the operation factor and the objective function can be achieved. In addition, the position of the extreme point and the operation condition optimization can be accomplished by this mode. All relevant experimental data regression analysis and mappings are performed using the "STATISTICA" and "Design Expert" statistical suite software. A second-order polynomial equation containing linear, quadratic and cross-product items was proposed to fit the dependent and independent variables. ANOVA and R^2 are applied to examine the model's suitability. A higher F-value illustrates that more of the variance is likely to be defined by the model and a small one indicates the variance is mainly attributed to noise. Furthermore, P value (Prob. > F) should be less than 0.05 to confirm the validity of the model and the importance of the items.

3.2.1 Results of Gloss (Y_1) Analysis

The sequential model sum of squares (SMSS) and degree of freedom of the linear, quadratic, 2FI (2 factor interaction), and cubic models are shown in Table 4.

Table 4 Sequential model sum of squares for gloss

Sources	Sum of Squares	Degree of freedom	Mean Square	F-value	P-value
Mean vs total	9835.7	1	9835.7		
Linear vs Mean	930.7	3	310.2	8.96	0.002
2FI vs Linear	105.8	3	35.3	1.03	0.426
Quadratic vs 2FI	190.2	3	63.4	3.19	0.105
Cubic vs Quadratic	118.5	4	29.6	66.8	0.014
Residual	0.89	2	0.44		
total	11181.7	16	698.9		

The linear model includes SMSS from sol-gel deliver pressure (X_1), air transport pressure (X_2), and displacement speed (X3). The 2FI model is made up of the X_1X_2, X_1X_3, and X_2X_3, while the items of X_1^2, X_2^2, and X_3^2 constitute the

Preprints (www.preprints.org) | NOT PEER-REVIEWED | Posted: 20 February 2019 doi:10.20944/preprints201902.0192.v1

quadratic model. The statistical results of Table 4 indicate that incorporating the cubic item cause the model to be aliased. Hence, the full second-order polynomial is established to regress the experimental data. In general, the lower the gloss, the better the anti-glare. Hence, we aim to obtain the experimental conditions of X_1, X_2, and X_3 to reveal minimal gloss value. If a coefficient of an item in the polynomial equation is negative, it means a positive contribution to the anti-glare property. Following the regression techniques, the regression model is expressed in equation (3). The ANOVA of equation (3) is summarized in Table 5. The F-value of the model reaches 33.8 with a P value of 0.0002, indicating the significance of this regressed model. To check the validity of the regression model, the F-value of the lack of fit is calculated as 52.5 with a P value larger than 0.05, indicating that the lack of fit is insignificant relative to pure error. The R^2 is calculated as 0.98, which is larger than the critical value of 0.8 to justify the adequacy of the regressed model [16] and indicate the experimental data

Table 5. Results of the regression model and ANOVA for gloss

Parameter	Parameter Estimate	Standard Error	95% CI Low	95% CI High
Intercept	25.617	2.971	18.346	32.887
X_1	9.079	2.282	6.287	11.872
X_2	-12.502	2.282	-15.295	-9.710
X_3	6.650	2.282	3.858	9.443
X_1X_2	-7.912	2.980	-11.559	-4.265
X_1X_3	2.212	2.980	-1.434	5.859
X_2X_3	1.687	2.980	-1.959	5.334
X_1^2	8.345	2.773	4.952	11.738
X_2^2	7.920	2.773	4.527	11.313
X_3^2	1.596	2.773	-1.797	4.989

Parameter	Sun of square (SS)	Degree of freedom (df)	Mean square (MS)	F ratio (F-value)	Probability (P-value)
X_1	1124.914	1	1124.914	63.303	0.00021*
X_2	2132.900	1	2132.900	120.02	0.00003*

Preprints (www.preprints.org) | NOT PEER-REVIEWED | Posted: 20 February 2019 doi:10.20944/preprints201902.0192.v1

X_3	603.541	1	603.541	33.963	0.00112*
X_1X_2	500.861	1	500.861	28.185	0.01809*
X_1X_3	39.161	1	39.161	2.203	0.06451
X_2X_3	22.781	1	22.781	1.282	0.08438
X_1^2	643.677	1	643.677	36.223	0.00094*
X_2^2	579.763	1	579.763	32.625	0.00124*
X_3^2	23.542	1	23.542	1.324	0.29352
Lock of fit	106.216	5	21.243	52.452	0.10443
Pure error	0.405	1	0.405		
Total SS	5520.300	15			

R^2=0.981, R^2_{adj} = 0.952, R^2_{pred} = 0.843, Adeq Precision = 18.3

are reasonably consistent with the regressed results. In addition, the predicted R^2 of 0.84 is reasonable agreement with the adjusted R^2 of 0.95. These results also support the adequacy of the regression model. Table 6 presents the estimates of coefficients, and their standard errors, 95% confidence interval low and high values.

Table 6. The measured optimal condition of lowest gloss and highest haze, and the predicted ones from Eqs. (3) and (5), respectively.

Items	X_1 (Kpa)	X_2 (Kpa)	X_3 (mm/sec)	Experimental Value		Predicted Value	ARE %
					Average		
Gloss (GU)	250	560	140	9.1 9.7 9.8	9.5	9.2	3.3
					Average		
Haze (%)	260	600	20	50.4 58.2 52.3	53.6	59.3	9.6

ANOVA exhibits that the three linear terms of X_1, X_2, and X_3 display significant impact on the gloss because their P values are all less than 0.05, with

Preprints (www.preprints.org) | NOT PEER-REVIEWED | Posted: 20 February 2019 doi:10.20944/preprints201902.0192.v1

among the most significant effect being air transport pressure (X_2) owing to the highest F-value and the lowest P-value. The reason is that the atomized particles are becoming finer, and scattering more light to reduce the gloss as the air transport pressure increases. In addition, the regression model also implies that decreasing sol -gel deliver pressure (X_1) and displacement speed (X_3) can reduce gloss and improve anti-glare property. Reducing sol-gel deliver pressure leads to a small quantity of sol-gel particles to de deposited, so that the displacement speed should be slowed down to increase the atomization particle coverage and uniform distribution.

In the quadratic items, X_1^2 and X_2^2 also reach significant level (P-value<0.05). With regard to the cross-terms, only the interaction effect of X_1X_2 reaches a significant level, which also implies sol-gel delivery pressure (X_1) and air transport pressure (X_2) cross-term will affect each other and reduce the gloss value, and the remaining cross-terms of X_1X_3 and X_2X_3 are below the significant level.

The significance of X_1X_2 can be interpreted as follow. When the quantity of the sol-gel deliver is large, if the gas transport is insufficient, then it cannot be effectively atomized, and is likely to form a thick transparent film. On the other hand, when the sol-gel deliver is small and the gas transport pressure is large, finer atomized particles can be expected, but they cannot effectively cover and uniformly distribute on the glass substrate. According to the ANOVA, the P-values of the X_1X_3, X_2X_3, and X_3^2 are larger than 0.1, therefore, these terms can be omitted from equation (3), and the regression equation can be simplified to equation (4).

$$Y_1 = 25.617 + 18.159X_1 - 25.005X_2 + 13.301X_3 - 15.825X_1X_2 + 4.425X_1X_3 + 3.375\ X_2X_3 + 16.691X_1^2 + 15.840X_2^2 + 3.192X_3^2 \quad (3)$$

$$Y_1 = 25.617 + 18.159X_1 - 25.005X_2 + 13.301X_3 - 15.825X_1X_2 + 16.691X_1^2 + 15.840X_2^2 \quad (4)$$

This second order polynomial regression equation is use to quantitatively describe the relationship between the gloss value and spray-operating parameters. The response surface map and contour map are depicted in Figure 9.

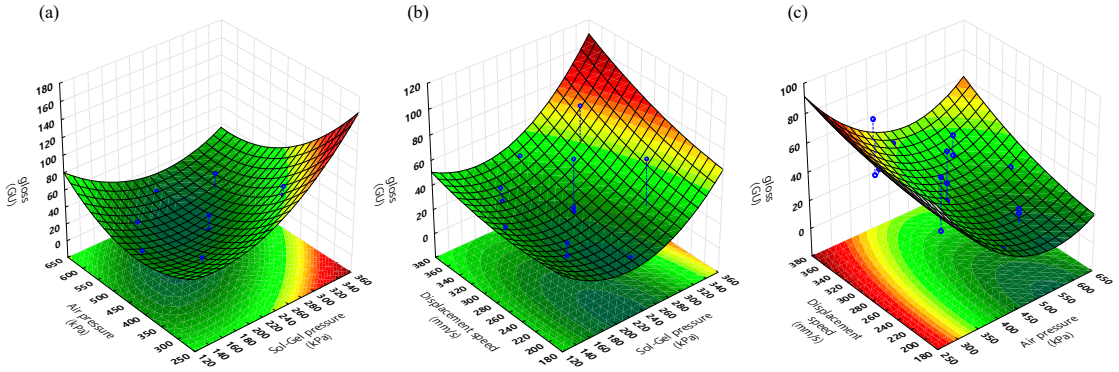

Preprints (www.preprints.org) | NOT PEER-REVIEWED | Posted: 20 February 2019 doi:10.20944/preprints201902.0192.v1

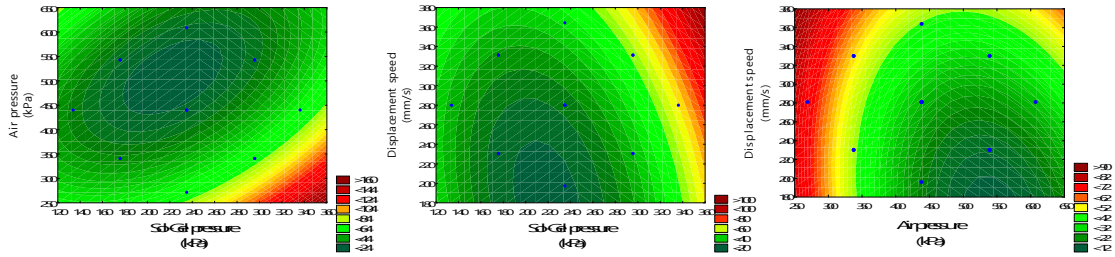

Figure 9. The response surface graph of the effect of (a)sol-gel deliver pressure and air transport pressure, (b)air transport pressure and displacement speed, and (c)displacement speed and air transport pressure.

According to Figure 9, the optimal (X_1, X_2, X_3) and gloss value are calculated as (250kPa, 560 kPa, 140 mm/s) and 9.2 GU. Furthermore, Figure 9 intuitively shows the effect of sol-gel deliver pressure, air transport pressure, and spray gun displacement speed on the gloss of the thin film samples. To verify the adequacy of the mathematical model, the experimental run at the optimal point was carried out. The averaged response gloss value is 9.5, with a negligible error of 3.3% when compared with the theoretical one.

3.2.2 Results of Haze (Y_2) Analysis

The haze value is also a vitally evaluated factor for the anti-glare property in industry. A higher haze implies the substrate surface is apt to fog, and then enhances the anti-glare peculiarity. Therefore, if the coefficient of each independent variable of the regressive model is positive, it means that it can positively contribute to anti-glare effect. The analysis of SMSS for haze is listed in Table 7. The quadratic model is suggested to be adopted to regress the experimental data because the cubic terms cause the model to be aliased. Following the regression procedure, the regression equation for haze is expressed as equation (5) using the coded-variables. The equation related to the actual values of variables is also shown in equation (6). Table 8 summarizes the results of ANOVA of the regressed model for haze.

Table 7 Sequential model sum of squares for haze

Sources	Sum of Squares	Degree of freedom	Mean Square	F-value	P-value
Mean vs total	10388.7	1	10388.7		

Preprints (www.preprints.org) | NOT PEER-REVIEWED | Posted: 20 February 2019 doi:10.20944/preprints201902.0192.v1

Linear vs Mean	943.6	3	314.5	12.87	0.0005
2FI vs Linear	85.7	3	28.6	1.24	0.3519
Quadratic vs 2FI	162.9	3	54.3	7.30	0.0199
Cubic vs Quadratic	42.7	4	10.7	11.1	0.0840 (aliased)
Residual	1.92	2	0.96		
total	11625.5	16	726.6		

The F-value of the model is 17.8 with a corresponding P-value of 0.0011, indicating the significance of this model. The R_2, R^2_{adj}, and R^2_{pred} are 0.964, 0.910, and 0.721. The predicted R^2 is in reasonable agreement with the adjusted R^2. These results also support the adequacy of the model. In addition, the F-value of the lack of fit is 17.6661 ($P > 0.05$), which indicated that it is not significant in responses due to the pure error and showed the adequacy of the model. From Table 8, the multiple regression and the variance (ANOVA) analysis, it can be seen that the sol-gel delivery pressure (X_1), air transport pressure (X_2) and displacement speed (X_3) all reach the significant level(P-value<0.05) in the linear terms, with among the most significant variables of air transport pressure (X_2) and displacement speed (X_3).

Table 8. Results of the regression model and ANOVA for haze

Parameter	Parameter Estimate	Standard Error	95% CI Low	95% CI High
Intercept	31.431	1.923	26.724	36.139
X_1	-2.736	0.738	-4.545	-0.930
X_2	5.992	0.738	4.187	7.803
X_3	-5.068	0.738	-6.878	-3.262
X_1X_2	2.775	0.964	0.4139	5.136
X_1X_3	-1.175	0.964	-3.536	1.186
X_2X_3	-1.275	0.964	-3.636	1.086
X_1^2	-2.443	0.896	-4.640	-0.247
X_2^2	-3.857	0.896	-6.057	-1.664
X_3^2	-0.675	0.896	-2.869	1.524

Parameter	Sun of square	Degree of freedom	Mean square	F ratio (F-value)	Probability (P-value)

Preprints (www.preprints.org) | NOT PEER-REVIEWED | Posted: 20 February 2019 doi:10.20944/preprints201902.0192.v1

	(SS)	(df)	(MS)		
Model	1192.124	9	132.458	17.803	0.0011*
X_1	102.293	1	102.293	13.733	0.0100*
X_2	490.483	1	490.483	65.849	0.0002*
X_3	350.788	1	350.787	47.094	0.0005*
X_1X_2	61.605	1	61.605	8.270	0.0281*
X_1X_3	11.045	1	11.045	1.482	0.2688
X_2X_3	13.005	1	13.005	1.745	0.2343
X_1^2	55.202	1	55.201	7.411	0.0344*
X_2^2	137.785	1	137.784	18.498	0.0051*
X_3^2	4.179	1	4.179	0.561	0.4796
Lock of fit	44.191	5	8.838	17.67	0.1787
Pure error	0.500	1	0.500		
Total SS	1236.764	15			

R^2=0.964, R^2_{adj} = 0.910, R^2_{pred} = 0.721, Adeq Precision = 13.9

The model also reflects that a slight increase in X_2 and a slight decrease in X_3 can produce more obvious increment in haze than that by a slight reduce in X_1 starting from the center point (0,0,0). The reason is that when an appropriate amount of sol-gel samples combined with adequate amount of gas to atomization, the atomized particle coverage and uniform distribution can be anticipated to increase if the displacement speed is slowed down. For the quadratic terms, X_1 and X_2 also reached a significant level (P-value < 0.05), which means that these two variables have quadratic effects on haze. Because the coefficients of X_1^2 and X_2^2 are negative, the extreme values of the haze with X_1 and X_2 are supposed to occur. With regard to the cross-terms, only the interaction effect between X_1 and X_2 reaches a significant level and exhibits a positive coefficient in the regression model for haze (P<0.05), which implies the X_1X_2 cross-term will affect each other and increase the haze value. The remaining cross-terms of X_1X_3 and X_2X_3 are below the significant level. Accordingly, the terms of X_1X_3, X_2X_3, and X_3^2 can be omitted from equations (5) and (6).

$$Y_2 = 31.43 - 2.74X_1 + 5.99X_2 - 5.07X_3 + 2.775X_1X_2 - 1.175X_1X_3 - 1.275X_2X_3$$

Preprints (www.preprints.org) | NOT PEER-REVIEWED | Posted: 20 February 2019 doi:10.20944/preprints201902.0192.v1

$$- 2.443X_1^2 - 3.857X_2^2 - 0.675X_3^2 \quad (5)$$

$$Y_2 = -98.71+0.181X_1 + 0.362X_2+0.255X_3 + 0.000463X_1X_2 - 0.00039X_1X_3 -$$

$$0.00026X_2X_3 - 0.00068X_1^2 - 0.00039X_2^2 - 0.00027X_3^2 \quad (6)$$

The response surface and contour maps are depicted in Figure 10.

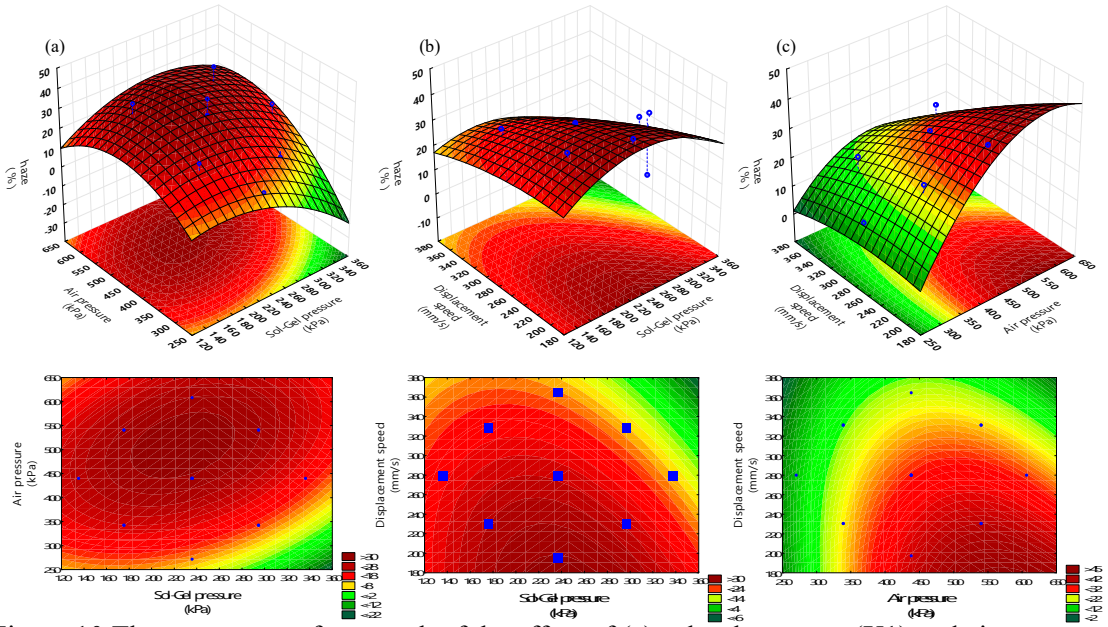

Figure 10 The response surface graph of the effect of (a) sol-gel pressure (X1) and air transport pressure (X2), (b) displacement speed (X3) and sol-gel deliver pressure (X1), (c)displacement speed (X3) and air transport pressure (X3).

Intuitively, Figure 10 shows the effect of sol-gel deliver pressure, air transport pressure, and spray gun displacement speed on the hazes of the anti-glare glass samples. According to Figure 10, the optimal haze is found as 59.3% with X_1, X_2, X_3 of 260 kPa, 600 kPa, and 20 mm/s, respectively, by following the optimal procedure. To examine the predicted ability of the mathematical model, we have conducted the experiments around the optimal point of X_1, X_2, X_3 of 260 kPa, 600 kPa, and 20 mm/s. The averaged response haze value is 53.6 %, which is very close to the theoretically predicted one of 59.3 %, with an error of 9.6 %. This result confirms the adequacy of the mathematical model. The experimental results are shown in Table 6.

4. Conclusion

Anti-glare glass can be prepared by a spray coating method using silica sol-gel material. The factors of sol-gel delivery (X_1) and air transport (X_2) pressure, and

displacement speed of spray gun (X_3) are proved to significantly affect the formation of anti-glare thin films. Increasing sol-gel deliver and air transport pressure, and reducing the displacement speed are favorable of reducing the gloss and raising the haze and transmittance, and then enhancing the anti-glare property. A statistical strategy based on response surface methodology is employed to optimize the spray-coating procedure. Furthermore, a quadratic polynomial equation is obtained and reasonably explains the relationship between the dependent variables (gloss and haze) and the independent variables (X_1, X_2, and X_3). The ANOVA analysis indicates that the gloss is significantly affect by the factors of X_1, X_2, X_3, X_1X_2, X_1^2, and X_2^2, while the haze is mainly influenced by X_1, X_2, X_3, X_1X_2, X_1^2, and X_2^2. The effect of X_1 and X_2 on anti-glare property is supposed to be superior to that of X_3. The RSM reveals the optimal points are around (250kPa, 560kPa, 140 mm/s) and (260kPa, 600, 20) to give the lowest gloss 9.2 GU and the highest haze 59.3%, respectively, which in turn results in the optimal anti-glare property. These theoretically predicted results are also verified by real experimental data, confirming the adequacy of the mathematical model.

Author Contributions

Y. H. Huang proposed the research topic, Y. H. Huang and L. C. Chen conceived and designed the experiments. Y. H. Huang performed the experimental work and statistical analysis, and wrote the original draft. L. C. Chen supervised the project, edited the manuscript, and contributed largely to the interpretation of the results. H. M. Chou supervised the research and provided direction.

References

[1] J. L. Cho, “Fabrication of omnidirectional anti-reflection coating with optimal spin-coating of silicon dioxide nanoparticle”, Yuan Ze University Optoelectronic Engineering Master's Thesis，2015。

[2] S. T. Tri Rakhmawati, “Dispersion of Colloidal Silica and Its Application to form a Light-Scattering Layer on Glass Substrates ”, Taiwan Tech Chemical Engineering Master's Thesis, 2012。

[3] X. K. Ma, N. H. Lee, H. J. Oh, J. W. Kim, C. K. Rhee, K. S. Park, S. J. Kim, “Surface Modification and Characterization of Highly Dispersed Silica Nanoparticles by a Cationic Surfactant”, Colloids and Surfaces A: Physicochem.

 doi:10.20944/preprints201902.0192.v1

Eng. Aspects, 358, **2010**, pp. 172-176.

[4] Glass Materials from Abrisa Technologies, "Soda-lime-Anti-glare reducing etched glass", http: // datasheets.globalspec.com / ds /1945 /AbrisaTechnologies / 52E6 A8C0-E687-4353-8EE4-74CFA76AA368

[5] H. Chen, L. Chen, H. Gong, L. Hong, C. C. Li, "Anti-glare substrates with a uniform textured surface and low sparkle and methods of making the same", WO2016069113A1, 2016.

[6] C. J. Brinker, G. W. Scherer, "Sol-Gel Science: The Physics and Chemistry of Sol-Gel Processing", 1990.

[7] L. C. Klein, "Sol-Gel Optics: Processing and Applications", 1994.

[8] E. Lugscheider, C. Barimani, P. Eckert and U. Eritt, Modeling of the APS plasma spray process, *Computational Materials Science*, 7(1996) 109-114.

[9] D. T. Santos, P. C. Veggi, M. A. A. Meireles, "Optimization and economic evaluation of pressurized liquid extraction of phenolic compounds from jabuticaba skins", Journal of Food Engineering, Vol. 108, 2012, pp. 444-452.

[10] L. Sun, S. Wan, Z. Yu, L. Wang, "Optimization and modeling of preparation conditions of TiO_2 nanoparticles coated on hollow glass microspheres using response surface methodology", Separation and Purification Technology, Vol.125,2014, pp.156-162.

[11] H. Kashudhan, A. Dixit and A. Upadhyay, "Optimization of ingredients for the development of wheatgrass based therapeutical juice using response surface methodology (RSM)", Journal of Pharmacognosy and Phytochemistry Vol.6(2), 2017, pp. 338-345.

[12] J.M. Hernandez-Vazquez, I. Garitaonandia, M.H. Fernandes, J. Muñoa, L.N.L. de Lacalle, "A Consistent Procedure Using Response Surface Methodology to Identify Stiffness Properties of Connections in Machine Tools". Materials **2018**, Vol.11(7), 2018, pp.1220.

[13] S. T. Hsu, L. C. Chen, C. C. Lee, T. C. Pan, B. X. You and Q. F. Yan, "Preparation of methacrylic acid-modif**ied** rice husk improved by an experimental design and application for paraquat adsorption". Journal of Hazardous Materials, Vol.171, 2009, pp. 465-470.

[14] R. Greashan and E. Inamine, "Nutritional improvement of process". Manual of industrial microbiology, 1986.

[15] G. E. P. Box and K. B. Wilson, "On the Experimental Attainment Optimum Conditions". Journal of the Royal Statistical Society. B13, 1951, pp.1-45.

[16] H. Rostamian, M.N. Lotfollahi, "New functionality for energy parameter of redlich-kwong equation of state for density calculation of pure carbon dioxide

 doi:10.20944/preprints201902.0192.v1

and ethane in liquid, vapor and supercritical phases Period". Periodica Polytechnica Chemical Engineering, Vol.60, 2016, pp. 93–97.

[17] Y. H. Huang, H. M. Chou and L. C. Chen, "Influence of alcoholic solvents on the anti-glare property of silica sol-gel thin films". International Conference on Innovation, Communication and Engineering, Hangzhou, Zhejiang, P.R. China., Nov 9-14, 2018, pp. C–76.